Journal of Mines, Metals and Fuels, *71(10): 1411-1423; 2023. DOI: 10.18311/jmmf/2023/35789*

Print ISSN : 0022-2755

Journal of Mines, Metals and Fuels

Contents available at: *www.informaticsjournals.com/index.php/jmmf*

The Onset of Instability in A Magnetohydrodynamic Channel Flow through Porous Media of Casson Fluid

D. L. Shivaraj Kumar[1]*, M. S. Basavaraj[2] and N. Kavitha[3]

[1]*Department of Mathematics, M. S. Ramaiah Institute of Technology (Affiliated to VTU), Bengaluru-560 054, Karnataka, India; dlshivaraj@gmail.com.*

[2]*Department of Mathematics, M. S. Ramaiah Institute of Technology(Affiliated to VTU), Bengaluru-560 054, Karnataka, India.*

[3]*Department of Mathematics, M. S. Ramaiah Institute of Technology(Affiliated to VTU), Bengaluru-560 054, Karnataka, India.*

Abstract

A detailed study is made on the stability of linear two-dimensional disturbances of Plane Poiseuille Flow (PPF) of Casson fluid through porous media in the presence of a vertical uniform magnetic field, which is extremely useful in metals, mines, and fuels industries. Using the method of normal modes, the disturbance equations are derived. The resulting eigenvalue problem is then solved by the spectral collocation method using Chebyshev-based polynomials. The critical values of the triplets (Re_c, α_c, c_c) are obtained for various values of the Casson parameter, η, Hartmann number, Ha, and porous parameter, σ_p. The stability of the system is discussed using the neutral stability curves for each value of the parameters present in the problem. It is found that the stability regions are enlarged for small values of η and large values of the porous parameter, σ_p and Hartmann number, Ha. It is also observed that the stability characteristics of plane Poiseuille flow in a porous medium are remarkably different from non-porous cases. The results obtained here contribute to the contemporary efforts to better understand the stability characteristics of PPF of Casson fluid flow through porous media in the presence of a uniform transverse magnetic field.

Keywords: *Eigenvalue Problem, Energy Method, Magnetohydrodynamics, Spectral Collocation Method*

1.0 Introduction

In the metals, mines, and minerals industries, fluid flow plays a critical role in processes such as ore extraction, transport, and refinement. Understanding the stability of these flows is essential for preventing disruptions and optimizing efficiency. Similarly, in the fuels industry, stability analysis is indispensable in ensuring the smooth and reliable transport of liquid fuels through pipelines and distribution networks. This research addresses the specific needs of these industries by shedding light on the stability characteristics of Casson fluid flow through porous media under the influence of a magnetic field. Such knowledge has the potential to revolutionize the design and operation of fluid systems within these sectors, resulting in enhanced reliability and efficiency.

In recent years, the study of fluid flow stability has captured the attention of scientific researchers, owing to its wide-ranging applications across various domains of applied engineering, including mechanical engineering, chemical engineering, meteorology, geophysics, astrophysics, atmospheric sciences, medical sciences, and

*Author for correspondence

biological systems. Understanding the stability of fluid flow is crucial for optimizing processes and systems in these fields.

Researchers have employed a plethora of numerical and analytical methods to tackle the complex equations that arise when addressing stability issues. The renowned Orr-Sommerfeld equation, which characterizes stability in fluid flows, has been a focal point of investigation. Valuable insights into these methods can be found in the works of Drazin[1], Tritton[2], Drazin[3], Criminale[4], and Chandrashekar[5]. Orszag[6], for instance, employed numerical solutions based on Chebyshev polynomial expansions and the QR matrix algorithm to determine a critical Reynolds number of 5772.22, marking the threshold at which flow stability is ensured. Chock[7] utilized the Runge-Kutta procedure, achieving remarkable accuracy through Chebyshev polynomial methods. Dowell[8] harnessed orthogonal function expansion to calculate a critical Reynolds number of 5750, demonstrating the reliability of these techniques. Similarly, Makinde[9] and Basavaraj[10] applied the Chebyshev collocation and Galerkin methods, respectively, both yielding accurate results. The Casson fluid model has emerged as a significant player in contemporary fluid dynamics research, driven by its relevance in various practical applications. Notably, this model has been applied to mathematically describe blood flow in narrow arteries under low shear rates, making it vital in medical and biological contexts. Mustafa[11], for instance, investigated the analytical solutions for unsteady flow and heat transfer of a Casson fluid, revealing that nondimensional time affects temperature positively while diminishing velocity. The magnetohydrodynamic (MHD) flow of Casson fluid through permeable stretching or shrinking sheets with mass transfer near walls has also been explored by Bhattacharyya[12]. Casson fluids with high yield stress, a non-Newtonian variant, have found widespread use in modeling blood flow in narrow arteries and have critical applications in polymer processing industries and biomechanics. Additionally, this rheological model proves suitable for characterizing blood and plasma behavior. Nadeem[13] and Fung[14] have highlighted its suitability for blood flow modeling, while Boyd[15] and Kandasamy[16] emphasize its applicability in plasma studies. Various models have been proposed to elucidate non-Newtonian fluid behavior and its extensive applications[17-20]. Remarkably, despite the substantial body of research in this field, there has been a notable gap in the exploration of instability in magnetohydrodynamic channel flow through porous media for Casson fluids.

Recent studies have contributed significantly to the understanding of Casson fluid behavior and its applications. Asogwa[21] explored the magnetohydrodynamic (MHD) Casson fluid flow over a stretching sheet while considering heat and mass transfer. This investigation provides insights into the complex interplay of magnetic fields, fluid dynamics, and thermal and mass transfer phenomena. Ridhwan[22] delved into the analytical solution of the impact of the Caputo-Fabrizio fractional derivative in the context of Casson fluid flow. This work extends our knowledge of the fundamental properties of Casson fluids and their fractional derivatives, which have practical implications in various applications. Saravana[23] and Eshwara Rao[24] conducted studies focusing on thermal radiation and diffusion effects in Casson flow. These investigations examine how heat and mass transfer interact with the unique rheological properties of Casson fluids, providing crucial insights for applications in heat exchangers, chemical processes, and environmental engineering. Tunde[25] examined the entropy generation in MHD Casson fluid flow, shedding light on the thermodynamic aspects of these flows, with implications for energy efficiency and process optimization. Kudenatti[26] addressed the temporal stability of linear Plane Poiseuille Flow (PPF) of Casson fluid with high yield stress in the presence of a magnetic field. This research offers valuable insights into the stability characteristics of Casson fluid flow, particularly in scenarios involving magnetic fields, which are relevant to various industrial applications. Kouz[27] and Santoshi[28] conducted numerical analyses of three-dimensional Casson fluid flow with constant heat flux, contributing to our understanding of the complex behavior of Casson fluids in real-world situations, such as chemical processing and heat transfer systems. These studies collectively enhance our knowledge of Casson fluid behavior and have practical implications across various fields of engineering and science.

To address this gap, our study aims to investigate the hydromagnetic stability of linear two-dimensional disturbances in Plane Poiseuille Flow (PPF) of Casson fluid through porous media in the presence of a vertical magnetic field. This research holds significant promise for the metals, mines, minerals, and fuels industries, where the control and optimization of fluid flow are pivotal to various processes and systems. In particular, the study

is expected to provide valuable insights into stability characteristics that can enhance the design and operation of fluid-related processes in these industries.

2.0 Formulation of the Problem

A systematic sketch of flow configuration and the coordinate axes can be found in Figure 1 which consists of an incompressible, electrically conducting non-Newtonian and inelastic Casson fluid flow between two infinitely long parallel rigid plates through a porous medium of width 2h. The flow is due to a constant pressure gradient in the flow direction. A constant magnetic field B_0 is applied along the transverse direction of the flow. The Cartesian coordinates are chosen such that the origin is in the middle of the channel, the x-axis is parallel to the flow direction, and the y-axis is directed vertically upward. The governing equations of the flow of non-Newtonian Casson fluid are:

$$\nabla.\vec{q} = 0\,, \qquad (1)$$

$$\frac{\rho}{\varepsilon}\left[\frac{\partial \vec{q}}{\partial t} + \frac{(\vec{q}.\nabla)\vec{q}}{\varepsilon}\right] = -\nabla p - \frac{\mu_D}{\kappa}\vec{q} + \mu_m\left(\vec{J}\times\vec{B}\right) + \nabla.\tau\,, \quad (2)$$

whereas the velocity having components (u, v), $\vec{B}$ is the magnetic field, ρ is the fluid density, p is the pressure, t is the time, μ_D is the dynamic viscosity, μ_m is the magnetic permeability, κ is the permeability, $\vec{J}$ is the current density, τ is stress tensor and ε is the porosity of porous medium.

The Lorentz force $\vec{J}\times\vec{B}$ is given by,

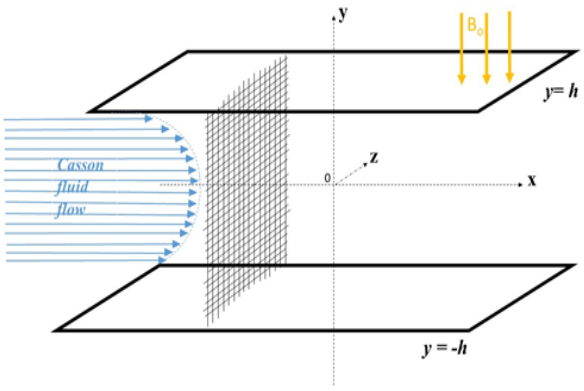

Figure 1. Schematic representation of problem considered.

$$\vec{J} = \sigma\mu_m\left(\vec{q}\times\vec{B}\right), \qquad \vec{q}\times\vec{B} = uB_0\hat{k}\,,$$

$$\left(\vec{J}\times\vec{B}\right) = \left(-\sigma\mu_m B_0^2 u\hat{i} + 0\hat{j} + 0\hat{k}\right), \qquad (3)$$

where σ is the electrical conductivity of the fluid.

The stress tensor τ for an isotropic and incompressible flow of a Casson fluid is

$$\tau_{ij} = \begin{Bmatrix} 2\left(\mu_e + \frac{\theta_y}{\sqrt{2\pi}}\right)e_{ij}, & if\ \pi > \pi_c \\ 2\left(\mu_e + \frac{\theta_y}{\sqrt{2\pi_c}}\right)e_{ij}, & if\ \pi < \pi_c \end{Bmatrix}. \qquad (4)$$

In the above expression $e_{ij} = \frac{1}{2}\left(\frac{\partial u_i}{\partial x_j} + \frac{\partial u_j}{\partial x_i}\right)$ is (i, j)th components of the rate of deformation, $\pi = e_{ij}e_{ij}$ is the product of deformation tensor with itself and π_c is the critical value of π based on the non-Newtonian model, μ_e is the Brinkman viscosity, θ_y is the yield stress,

Then we get,

$$e_{xx} = \left(\frac{\partial u}{\partial x}\right), \qquad e_{yy} = \left(\frac{\partial y}{\partial y}\right), \qquad e_{zz} = \left(\frac{\partial w}{\partial z}\right),$$

$$e_{xy} = e_{yx} = \frac{1}{2}\left(\frac{\partial u}{\partial y} + \frac{\partial v}{\partial x}\right), e_{xz} = e_{zx} = \frac{1}{2}\left(\frac{\partial u}{\partial z} + \frac{\partial w}{\partial x}\right),$$

$$e_{yz} = e_{zy} = \frac{1}{2}\left(\frac{\partial v}{\partial z} + \frac{\partial w}{\partial y}\right).$$

Equation 4 represents the non-Newtonian fluid with solid-like behavior with high yield stress. The flow of Casson fluid is obtained if the applied stress is more than that of critical value But we are considering the non-Newtonian Casson fluid behavior to study the linear stability of magnetohydrodynamic fluid flow through a porous medium with a uniform transverse magnetic field.

The modified version of the above empirical relation is employed by Fusi[29], M Nawaz[30].

The stress tensor components are

$$\tau_{xx} = 2\mu_e\left(1 + \frac{1}{\eta}\right)\frac{\partial u}{\partial x}, \tau_{yy} = 2\mu_e\left(1 + \frac{1}{\eta}\right)\frac{\partial v}{\partial y},$$

$$\tau_{zz} = 2\mu_e\left(1+\frac{1}{\eta}\right)\frac{\partial w}{\partial z}.$$

$$\tau_{xy} = \tau_{yx} = \mu_e\left(1+\frac{1}{\eta}\right)\left(\frac{\partial u}{\partial y}+\frac{\partial v}{\partial x}\right),$$

$$\tau_{xy} = \tau_{yx} = \mu_e\left(1+\frac{1}{\eta}\right)\left(\frac{\partial u}{\partial y}+\frac{\partial v}{\partial x}\right),$$

$$\tau_{yz} = \tau_{zy} = \mu_e\left(1+\frac{1}{\eta}\right)\left(\frac{\partial v}{\partial z}+\frac{\partial w}{\partial y}\right),$$

The stress tensor becomes,

$$\tau_{ij} = \mu_e\left(1+\frac{1}{\eta}\right)\begin{bmatrix} 2\left(\frac{\partial u}{\partial x}\right) & \left(\frac{\partial u}{\partial y}+\frac{\partial v}{\partial x}\right) & \left(\frac{\partial u}{\partial z}+\frac{\partial w}{\partial x}\right) \\ \left(\frac{\partial u}{\partial y}+\frac{\partial v}{\partial x}\right) & 2\left(\frac{\partial v}{\partial y}\right) & \left(\frac{\partial v}{\partial z}+\frac{\partial w}{\partial y}\right) \\ \left(\frac{\partial u}{\partial z}+\frac{\partial w}{\partial x}\right) & \left(\frac{\partial v}{\partial z}+\frac{\partial w}{\partial y}\right) & 2\left(\frac{\partial w}{\partial z}\right) \end{bmatrix}, \quad (5)$$

with $\eta = \frac{\mu_e\sqrt{2\pi_c}}{\theta_y}$ being the Casson parameter.

3.0 Basic Flow

The steady-state flow of Casson fluid is fully developed, unidirectional and is driven only by a constant pressure gradient that is $\vec{q} = \vec{q}_b = [u_b(y), 0, 0]$.

At a steady state, the stress tensor becomes

$$\tau_{ij} = \mu_e\left(1+\frac{1}{\eta}\right)\begin{bmatrix} 0 & \left(\frac{du}{dy}\right) & 0 \\ \left(\frac{du}{dy}\right) & 0 & 0 \\ 0 & 0 & 0 \end{bmatrix}.$$

Nondimensionalisation is carried out by using the non-dimensional quantities denoted through over bars,

$$(\bar{u}, \bar{v}, \bar{w}) = \frac{(u, v, w)}{U_0},$$

$$\bar{\nabla} = h\nabla,$$

$$\bar{t} = \frac{t}{h\varepsilon / U_0},$$

$$\bar{P} = \frac{p}{\rho U_0^{\,2} / \varepsilon^2},$$

$$(\bar{x}, \bar{y}, \bar{z}) = \frac{(x, y, z)}{h},$$

where U_0 is average velocity, ρ is fluid density, h is the half channel length.

Then by neglecting the upper bars we get,

$$\frac{dP}{dx}Re = \frac{d^2u_b(y)}{dy^2}S - Ha^2u_b(y) - \sigma_p^2u_b(y), \quad (6)$$

$$u_b(y) = 0 \; at \; y \pm 1. \quad (7)$$

Here, $Re = \frac{U_0h\rho}{\mu_e\varepsilon^2}$ is the Reynolds number, $Ha = hB_0\sqrt{\frac{\sigma}{\mu}}$ is the Hartmann number, $\sigma_p = h\sqrt{\frac{\mu_D}{\mu_e k}}$ is the modified porous parameter, Let $S = \left(1+\frac{1}{\eta}\right)$, $\chi = \frac{\sqrt{\mathrm{Ha}^2 + \sigma_p^{\,2}}}{\sqrt{S}}$, $\bar{\bar{P}} = -\frac{dP}{dx}Re$ is dimensionless pressure gradient satisfy the normalisation condition $u_b(y) = 1$ then the solution of Equation (6) is given by

$$u_b(y) = -\frac{\bar{\bar{P}}}{Ha^2}\frac{1}{(e^{2\chi}+1)}e^{-\chi y}\left(e^{\chi} - e^{\chi y} - e^{2\chi+\chi y} + e^{\chi+2\chi y}\right). \quad (8)$$

That is,

$$u_b(y) = \frac{\bar{\bar{P}} - \bar{\bar{P}}cosh(\chi y)sech(\chi)}{Ha^2 + \sigma_p^{\,2}}. \quad (9)$$

By using centre-line velocity, we get

$$\bar{\bar{P}} = \frac{1}{2}\left[2 + \cos ech\left(\frac{\chi}{2}\right)^2\right]\left(\mathrm{Ha}^2 - \sigma_p^{\,2}\right), \quad (10)$$

$$u_b(y) = \frac{cosh(\chi) - cosh(\chi y)}{cosh(\chi) - 1}. \quad (11)$$

Which is the expression for the velocity distribution of PPF of a considered Casson fluid.

Limiting Cases: -

The solution for the fluids with large viscosity:

$$\lim_{\eta\to\infty} u_b(y) = \frac{\cosh(\sqrt{Ha^2+\sigma_p^{\,2}}) - \cosh(\sqrt{Ha^2+\sigma_p^{\,2}}\,y)}{\cosh(\sqrt{Ha^2+\sigma_p^{\,2}}) - 1} \quad . \qquad (12)$$

Similarly,

$$\lim_{\substack{Ha\to 0\\ \eta\to\infty}} u_b(y) = \frac{\cosh(\sigma_p) - \cosh(\sigma_p y)}{\cosh(\sigma_p) - 1} \qquad (13)$$

Which is corresponding to the results of Nield[31], Hill[32] and Shankar[10].

The solution for clear fluid is,

$$\lim_{\substack{\sigma_p\to 0\\ \eta\to\infty}} u_b(y) = \frac{\cosh(Ha) - \cosh(Ha\,y)}{\cosh(Ha) - 1} \, . \qquad (14)$$

Which corresponds to the results of Takashima[34] and also for

$$\lim_{\substack{Ha\to 0\\ \sigma_p\to 0\\ \eta\to\infty}} u_b(y) = 1 - y^2 \, . \qquad (15)$$

Figure 2a represents the plots of steady-state velocity profiles $u_b(y)$ by taking fixed Casson parameter η = 1 for different values of Hartmann number Ha without porous media. It clearly presents the effects of the Hartmann number on the basic flow. The velocity curves start increasing from $y = -1$ and reaches maximum at the centre line of the channel at y = 0 and decrease from there and reach zero at $y = 1$. The velocity starts exponentially

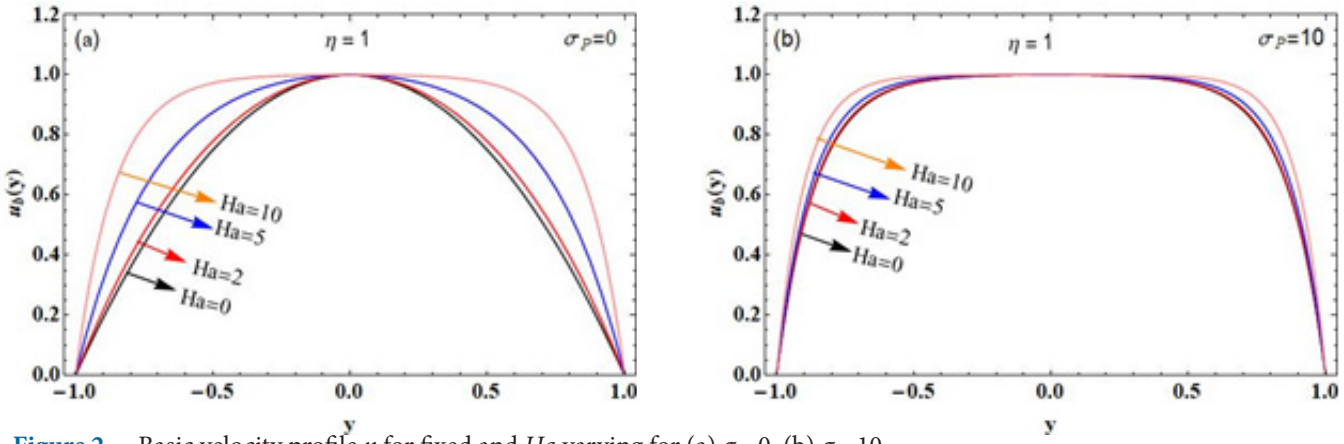

Figure 2. Basic velocity profile η for fixed and Ha varying for (a) σ_p=0, (b) σ_p=10.

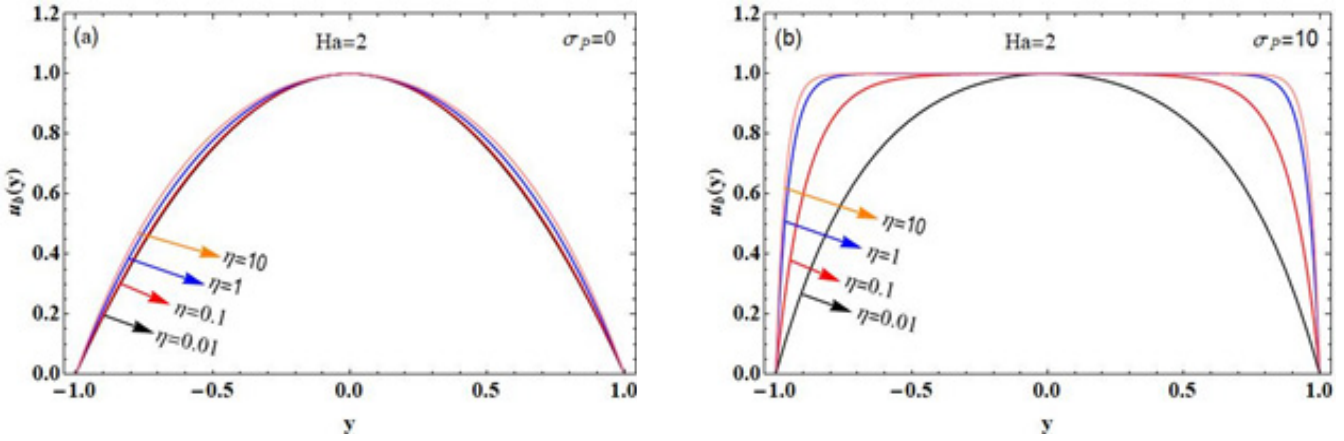

Figure 3. Basic velocity profile for fixed Ha and varying η for (a) σ_p=0, (b) σ_p=10.

from $y=-1$ with a simultaneous increase in the Hartmann number and then takes parabolic form by the way they reach the end at $y=1$. The velocity increases significantly with an increase in the Hartmann number and becomes slower towards the end. Thereby, one can see a region of slow fluid flow for larger values of the Hartmann number relatively one can see a region of fast fluid flow with smaller values of the Hartmann number. The results are comparable with the results of Takashima[33] and Lock[34]. With a highly porous medium Figure 2b, one has not seen great variation in velocity but there is sight similar trend.

Figure 3a represents the plots of steady-state velocity profiles by $u_b\ (y)$ by taking constant Hartmann number *Ha* for different values of the Casson parameter η. In the absence of a porous medium, the velocity curves are starting increases from y = -1 and reaches a maximum at the centre line of the channel at y = 0 and decreases from there and reaches zero at y = 1 with a parabolic shape, a small variation in velocity is observed while the Casson parameter increased. But very significant change in velocity is observed with high porous parameter (σ_p=10) That is by an increase of Casson parameter ηand, the velocity profile takes parabolic form from y = -1 to y = 1 with slower fluid flow near boundaries in Figure 3b. Clearly increase in porous parameters adversely affects the velocity of the fluid near boundaries.

4.0 Stability Analysis

Linear stability analysis of the electrically conducting Casson fluid is carried out by taking infinitesimal disturbances to the basic state variables as,

$$(u,v,p,\tau)=(u_b(y),0,p,\tau)+(\bar{u},\bar{v},\bar{p},\bar{\tau})(x,y,t)\,. \quad (17)$$

where perturbation of stress tensor is taken as,

$$\tau_{ij}=\mu_e S\begin{bmatrix} 0 & \frac{du}{dy} & 0 \\ \frac{du}{dy} & 0 & 0 \\ 0 & 0 & 0 \end{bmatrix},$$

$$\bar{\tau}_{ij}=\mu_e S\begin{bmatrix} 2\frac{\partial\bar{u}}{\partial x} & \frac{\partial\bar{u}}{\partial y}+\frac{\partial\bar{v}}{\partial x} & 0 \\ \frac{\partial\bar{u}}{\partial y}+\frac{\partial\bar{v}}{\partial x} & 2\frac{\partial\bar{v}}{\partial y} & 0 \\ 0 & 0 & 0 \end{bmatrix},$$

$$\tau_{ij}+\bar{\tau}_{ij}=\mu_e S\begin{bmatrix} 2\frac{\partial\bar{u}}{\partial x} & \frac{du}{dy}+\frac{\partial\bar{u}}{\partial y}+\frac{\partial\bar{v}}{\partial x} & 0 \\ \frac{du}{dy}+\frac{\partial\bar{u}}{\partial y}+\frac{\partial\bar{v}}{\partial x} & 2\frac{\partial\bar{v}}{\partial y} & 0 \\ 0 & 0 & 0 \end{bmatrix} \quad (18)$$

Equation (1) and Equation (2) can be linearized using the steady-state solution (8). The arbitrary disturbance quantities are denoted by an upper bar.

By using the Fourier mode expansion

$$(\bar{u},\bar{v},\bar{p},\bar{\tau})(x,y,t)=(\bar{u},\bar{v},\bar{p},\bar{\tau})(y)e^{i(\alpha x-\omega t)}\,, \quad (19)$$

where α is the wavenumber in the x-direction, ω is the frequency and c is complex wave speed.

$$c=\frac{\omega}{\alpha}=c_r+ic_i \quad (20)$$

As α is positive (real quantity), the disturbances are amplified or damped depending on the sign of the imaginary part of c which is positive or negative. The disturbance is neutrally stable if the imaginary part of c is zero.

Then finally we obtain the stability equations as

$$D\bar{v}+i\alpha\bar{u}=0\,, \quad (21)$$

$$i\alpha(u_b(y)-c)\bar{u}+\bar{v}\,Du_b(y)=-i\alpha\bar{p}+\frac{S}{Re}(D^2-\alpha^2)\bar{u}-\frac{Ha^2}{Re}\bar{u}-\frac{\sigma_p^2}{Re}\bar{u}$$

, (22)

$$i\alpha(u_b(y)-c)\bar{v}=-D\bar{p}+\frac{S}{Re}(D^2-\alpha^2)\bar{v}-\frac{\sigma_p^2}{Re}\bar{v} \quad , \quad (23)$$

and the boundary conditions are

$$\bar{u}(\pm1)=0=\bar{v}(\pm1)\,. \quad (24)$$

5.0 Normal Modes

A Normal mode analysis is carried out by introducing stream functions that satisfy the continuity Equation (1)

$$\bar{u} = \frac{\partial \Psi}{\partial y}, \quad \bar{v} = -\frac{\partial \Psi}{\partial x} \quad \text{where} \quad \Psi(x,y,t) = Y(y)e^{i(\alpha x - \omega t)}$$

Equations (21), (22), (23), and (24) are reduced into the fourth-order Orr Sommerfeld type equation.

The wavenumber α is real so that the solution becomes bounded and $c = c_r + c_i$ is complex wave speed. Therefore, the given system is neutrally stable if $c_i = 0$ and unstable if $c_i > 0$, asymptotically stable $c_i < 0$.

$$\left(S(D^2-\alpha^2)^2 Y - Ha^2 D^2 \mathrm{Y} - \sigma_p^2 (D^2-\alpha^2)Y\right)\frac{1}{i\alpha Re} -$$

$$-u_b(y)(D^2-\alpha^2)Y + D^2 u_b(y)\mathrm{Y} = -c(D^2-\alpha^2)Y \qquad (25)$$

Which is the required fourth-order disturbance equation. The no-slip boundary conditions are,

$Y = 0 \;\; at \;\; y = \pm 1$.

6.0 Energy Analysis

An analytical energy method has been used to obtain the suitable sufficient condition for the stability of PPF of Casson fluid with arbitrary disturbances as follows.

Let $\overline{Y}$ be the conjugate of Y, then integrate the resulting equation over the flow domain y by taking the product with its conjugate $\overline{Y}$ in each term (Drazin et al.[1]) then we get,

$$\int_{-1}^{1}\left(S(|\mathrm{Y}''|^2 + 2\alpha^2|\mathrm{Y}'|^2 + \alpha^4|\mathrm{Y}|^2) + Ha^2|\mathrm{Y}'|^2 + \sigma_p^2|\mathrm{Y}'|^2 + \alpha^2|\mathrm{Y}|^2\right)dy =$$

$$\alpha Re\int_{-1}^{1}(\bar{\mathrm{Y}}(\mathrm{Y}''-\alpha^2\mathrm{Y})u_b(y) + \bar{\mathrm{Y}}(u_b''(y)\mathrm{Y}))dy + i\alpha cRe\int_{-1}^{1}(|\mathrm{Y}'|^2 + \alpha^2|\mathrm{Y}|^2)dy \qquad (26)$$

Equating real parts on both sides, we get

$$c_i = \frac{1}{\alpha Re\int_{-1}^{1}(|\mathrm{Y}'|^2 + \alpha^2|\mathrm{Y}|^2)dy}\int_{-1}^{1}\left(S(|\mathrm{Y}''|^2 + 2\alpha^2|\mathrm{Y}'|^2 + \alpha^4|\mathrm{Y}|^2)\right.$$

$$\left. + Ha^2|\mathrm{Y}'|^2 + \sigma_p^2|\mathrm{Y}'|^2 + \alpha^2|\mathrm{Y}|^2\right)dy \qquad (27)$$

If the Real part of $\mathrm{Y} = \mathrm{Y}_r$ an Imaginary part of $\mathrm{Y} = \mathrm{Y}_i$ then,

$$\frac{S}{\alpha Re}\int_{-1}^{1}(|\mathrm{Y}''|^2 + 2\alpha^2|\mathrm{Y}'|^2 + \alpha^4|\mathrm{Y}|^2)dy + \frac{Ha^2}{\alpha Re}\int_{-1}^{1}|\mathrm{Y}'|^2 +$$

$$\frac{\sigma_p^2}{\alpha Re}\int_{-1}^{1}|\mathrm{Y}'|^2\,dy + \frac{\alpha^2}{\alpha Re}\int_{-1}^{1}|\mathrm{Y}|^2 dy = E_r + iE_i \qquad (28)$$

where

$$E_r = \int_{-1}^{1}((\mathrm{Y}_r\mathrm{Y}_i' - \mathrm{Y}_i\mathrm{Y}_r')u'(y) - c_i(|\mathrm{Y}'|^2 + \alpha^2|\mathrm{Y}|^2))dy \qquad (29)$$

$$E_i = \int_{-1}^{1}((\mathrm{Y}_r\mathrm{Y}_r' + \mathrm{Y}_i\mathrm{Y}_i')u_b'(y) + c_r(|\mathrm{Y}'|^2 + \alpha^2|\mathrm{Y}|^2) -$$

$$(u_b(y)|\mathrm{Y}'|^2 + (u_b''(y) + \alpha^2)|\mathrm{Y}|^2))dy \qquad (30)$$

Let G denotes the LHS of (22),

By equating imaginary parts on both sides, we obtain the below expression which denotes the growth rate

$$c_i = \frac{1}{\int_{-1}^{1}(|\mathrm{Y}'|^2 + \alpha^2|\mathrm{Y}|^2)dy}\int_{-1}^{1}(\mathrm{Y}_r\mathrm{Y}_i' - \mathrm{Y}_i\mathrm{Y}_r')u_b'(y) - \frac{G}{\alpha Re}dy$$

By equating real parts on both sides, we obtain the below expression which denotes the phase velocity, (31)

$$c_r = \frac{1}{\int_{-1}^{1}(|\mathrm{Y}'|^2 + \alpha^2|\mathrm{Y}|^2)dy}\int_{-1}^{1}((\mathrm{Y}_r\mathrm{Y}_r' + \mathrm{Y}_i\mathrm{Y}_i')u_b'(y) +$$

$$u_b(y)|\mathrm{Y}'|^2 + (u_b''(y) + \alpha^2)|\mathrm{Y}|^2)dy \qquad (32)$$

Further,

$$\int_{-1}^{1}(\mathrm{Y}_r\mathrm{Y}_i' - \mathrm{Y}_i\mathrm{Y}_r')u_b'(y) =$$

$$\frac{i}{2}\int_{-1}^{1}(\mathrm{Y}\overline{\mathrm{Y}'} - \bar{\mathrm{Y}}\mathrm{Y}')u_b'(y) \le \int_{-1}^{1}|\mathrm{Y}||\mathrm{Y}'||u_b'(y)|\,dy \qquad (33)$$

$$\int_{-1}^{1}|\mathrm{Y}||\mathrm{Y}'||u_b'(y)|\,dy \le \int_{-1}^{1}|\mathrm{Y}|^2\,dy\int_{-1}^{1}|\mathrm{Y}'|^2\,dy(\max_{-1\le y\le 1}|u_b'(y)|)$$

(Schwartz's inequality) (34)

then the growth rate for the upper bound is

$$c_i = \frac{1}{\int_{-1}^{1}(|Y'|^2 + \alpha^2 |Y|^2)dy}\int_{-1}^{1}|Y|^2|Y'|^2\, dy(\max_{-1\le y\le 1}|u_b'(y)|) - \frac{G}{\alpha Re} \tag{35}$$

We get the sufficient expression on Re for stability as

$$Re < \frac{G}{\int_{-1}^{1}|Y|^2|Y'|^2\, dy(\alpha \max_{-1\le y\le 1}|u_b'(y)|)\int_{-1}^{1}(|Y'|^2 + \alpha^2|Y|^2)dy} \tag{36}$$

Equations (27) and (3) give the integral expressions for both c_i and Re which show the flow is stable at all values of parameters This is in contradiction to the experimental observations done by many researchers therefore, It is important to solve the stability equations (21) to (24) of the present system for more accurate values of the wavenumber α and Reynolds number Re .

7.0 Method of Solution

The numerical solution to the resulting fourth-order eigenvalue problem can be obtained using the Spectral methods (or transform methods) by taking Chebyshev polynomials as a base.

The interpolating polynomials for calculating the non-periodic functions at Chebyshev points are given by $y_j = cos(j\pi / N)$ for j = 0,1,2…. N.

The Chebyshev points are having irregular distribution and are clustered near boundaries at y = ±1. The Chebyshev polynomial, $T_k(y)$, where k represents the degree of the polynomial is used to approximate its function and its derivatives above Chebyshev points.

The k[th] degree Chebyshev polynomial is defined as,

$$T_k(y) = \cos(k\cos^{-1} y) = \cos(k\theta) \tag{37}$$

Then,

$$T_0(y) = 1,\ T_1(y) = y,\quad T_2(y) = 2y^2 - 1,\quad T_3(y) = 4y^3 - 3y$$

and so, on up to

$$T_{k+1}(y) = 2yT_k(y) - T_{k-1}(y) \quad k \ge 1 \tag{38}$$

Which are having N number of zeros in the interval [-1,1]. Then,

$$y_j = cos(\pi(j-1/2)/N),\quad j = 1, 2, \ldots, N$$

By using the above relations and also

$$u(y_j) = \sum_{k=0}^{N} a_k T_k(y_j)$$

where a_k be the coefficient of k[th] Chebyshev polynomial given by

$$a_k = \frac{2}{Nc_k}\sum_{j=0}^{N}\frac{1}{c_j}T_k(y_j)u_j,\quad k = 0,1,2,.....N$$

with $c_j = \begin{Bmatrix} 2 & if\ j = 0, N \\ 1 & otherwise \end{Bmatrix}$ i.e., $a = \hat{T}u$

Similarly, to obtain derivatives $u'(y_j) = \sum_{k=0}^{N} b_k T_k(y_j)$ i.e., $u' = Tb$ then stability equations are written into the form of the Chebyshev polynomials.

The matrix T and $\hat{T}$ are Chebyshev polynomials, then (N+1)× (N+1) be the Chebyshev collocation differential matrix, i.e., s_{jk} given by

$$s_{00} = \frac{2N^2+1}{6},\qquad s_{NN} = -\frac{2N^2+1}{6}$$

$$s_{ij} = \frac{-y_j}{2(1-y_j)^2},\quad j = 1,2,3,.....,(N-1)$$

$$s_{jk} = \frac{c_j(-1)^{i+k}}{c_k(y_j - y_k)},\quad j \ne k,\ j,k = 0,1,2,.....,N$$

By following the above steps, the generalized eigenvalue problem has been obtained. By using the QZ algorithm (Moler and Steward[35]) the eigenvalue problem can be solved by using suitable environmental tools.

The higher-order derivatives can be easily obtained by using their corresponding powers i.e., $u'' = D^2u,\ u''' = D^3u,\ u'''' = D^4u$.

8.0 Results and Discussion

By solving the generalized eigenvalue problem, the values of various parameters involved in the problem are calculated using the QZ algorithm. The marginal stability curves are plotted for a deeper understanding of the PPF

of a Casson fluid with a transverse magnetic field through porous media.

The results obtained in Table 1 are found to be accurate with the results obtained by Takashima[33]. By increasing the Hartmann number value, the method converged slowly in a non-porous case with the Casson parameter $\eta \to \infty$. This clearly shows that convergence becomes slower as *Ha* increases.

The effect of the Casson parameter η on critical values of the triplets (Re_c, α_c, c_c) are obtained with a uniform transverse magnetic field ($Ha = 1$) in a non-porous media ($\sigma_p = 0$) in Table 2 and the results are accurate with the results of Kudenatti *et al.*[26]. By increasing the value of the Casson parameter, the critical Reynolds number *Re* , the critical wavenumber α_c and the critical wave speed c_c found to decrease gradually. It is clear that from Table 2 the growth of the disturbances in Casson fluid is found to be increasing in the presence of a magnetic field compared to the corresponding ordinary Newtonian fluid.

By using the Chebyshev collocation method for linear stability of a PPF of a Casson fluid, the Neutral stability curves for various values have been plotted in (Re - α) plane.

Figure 4a represents the neutral stability curves for various values of Hartmann number *Ha* with Casson parameter $\eta \to \infty$ in (Re - α) plane. Each marginal stability curve is having an upper concave shape. The region of stable mode seems to be increasing by the simultaneous increase of critical Reynolds number Re_c but the corresponding critical wavenumber α_c shifting towards left in each curve. A higher range of stability can be achieved with an increase of *Ha* . That is the onset of

Table 1. Critical values of the triplets (Re_c, α_c, c_c) for various values of *Ha* when Casson parameter $\eta \to \infty$ and $\sigma_p = 0$.

		Takashima[33]			Present study		
N	*Ha*	Re_c	α_c	c_c	Re_c	α_c	c_c
30	0.0	5772.2218	1.02054	0.264000	5772.2256	1.02054	0.262000
30	0.5	6706.0911	1.00573	0.255883	6706.0111	1.00573	0.245883
35	1.0	10016.262	0.97192	0.235519	10016.264	0.97192	0.225519
40	2.0	28603.639	0.92777	0.192133	28603.662	0.92277	0.192133
45	3.0	65155.210	0.95824	0.169030	65155.293	0.95824	0.165030
55	4.0	112394.81	1.03545	0.159826	112394.81	1.03545	0.159826
60	5.0	164089.99	1.13424	0.156427	164089.94	1.13424	0.156321
65	6.03	219473.30	1.24715	0.155209	219473.35	1.24715	0.155200
75	7.64	308291.01	1.43718	0.154761	308291.89	1.43018	0.154650
85	10.0	439818.16	1.73914	0.154789	439818.23	1.73814	0.154773
90	11.29	510959.88	1.91502	0.154844	518959.32	1.91502	0.154840
100	15.0	708962.18	2.45660	0.154957	708962.43	2.45660	0.154949
120	20.0	961767.17	3.23764	0.155011	968767.21	3.23764	0.155012
140	30.0	1449060.2	4.84609	0.155028	1449060.0	4.84509	0.155028
180	50.0	2415550.1	8.07657	0.155029	2415550.2	8.02657	0.155029
210	70.0	3381771.1	11.3071	0.155029	3381541.1	11.3071	0.155029
250	100.0	4831101.5	16.1531	0.155029	4831323.5	16.2431	0.155029
360	200.0	9662203.3	32.3063	0.150029	9672321.3	32.3023	0.150029

Table 2. Critical values of the triplets (Re_c, α_c, c_c) for various values of Casson parameter η when a porous parameter $\sigma_p = 0$ (non-porous case) and $Ha = 1$.

η	α_c	Re_c	c_c
0.1	1.014285	67118.491945	0.260889
0.2	1.009814	38310.439037	0.258435
0.5	0.999996	21111.399265	0.253194
0.8	0.996041	16859.154274	0.250109
1.0	0.993115	15454.828316	0.248494
5.0	0.977857	11061.789468	0.239537
10	0.974642	10534.555496	0.237637
10^2	0.972722	10067.702366	0.235807
10^3	0.971421	10021.438171	0.235496
10^4	0.972142	10016.811887	0.235553
10^5	0.972142	10016.336031	0.235551

instability of magnetohydrodynamic flow is postponed with an increase in Hartmann number.

Figure 4b represents the marginal stability curves for various values Casson parameter η in the presence of magnetic field ($Ha = 1$) in (Re - α) plane. As a contrast to Figure 4a the critical value of the Reynolds number Re_c decreases with an increase in the value of the Casson parameter in each curve. For each neutral stability curve, the stable mode tends to decrease as the highest stable region can be seen with $\eta = 0.1$. That is the onset of instability of MHD flow is preponed with the increase in the Casson parameter.

For the various values of porous parameter σ_p in the presence of uniform magnetic field ($Ha = 1$) with fixed Casson parameter η = 5 various critical values of the triplets (Re_c, α_c, c_c) are obtained in Table 3. It is clearly shown that an increase in porous parameters gradually makes the system linearly stable by simultaneously increasing the critical Reynolds number which can be also visualized in Figure 5. Clearly, an increasing porous parameter dampens the infinitesimal disturbances and this is due to a decrease in the permeability of the porous media. That is, a clear characteristic of Casson fluid to delay the onset of instability can be seen with an increase in porous parameters. Thereby, both Hartmann number Ha and porous parameter σ_p will have the same effect on Casson fluid. But the porous parameter σ_p shows a slightly higher region of stabilization comparatively. Further increase in their values linearly stabilizes the system by postponing the onset of instability.

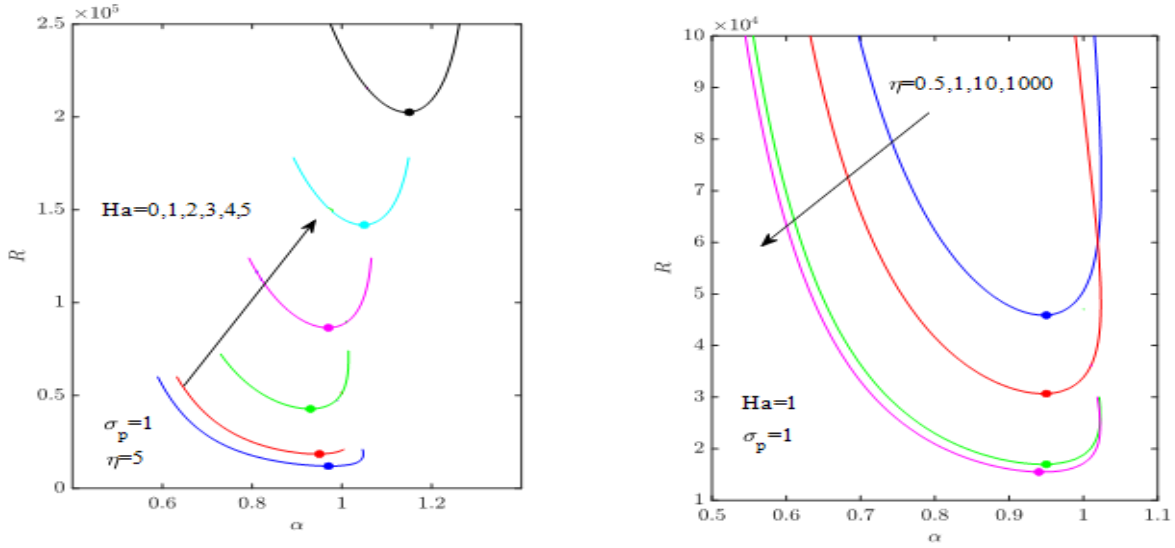

Figure 4. Neutral stability curves (a) varying Ha for $\eta \to \infty$ (b) varying η at $Ha = 1$

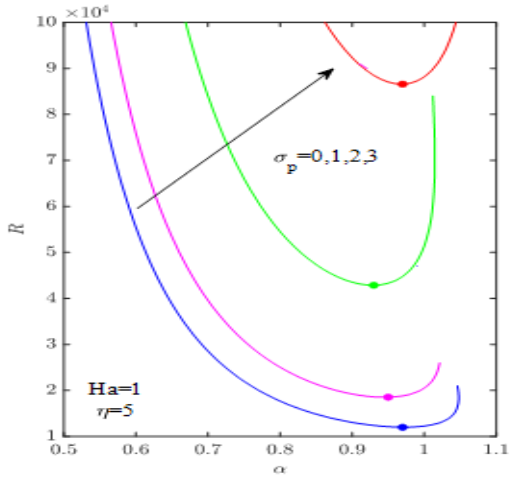

Figure 5. Marginal stability curves in (Re vs α) plane for different values of σ_p with $Ha = 1$ and $\eta = 5$.

Table 3. Critical values of the triplets (Re , α_c , c_c) for various values of porous parameter σ_p

[Present study] $Ha = 1, \eta = 5$			
σ_p	α_c	Re_c	c_c
0	0.9783	11999.766	0.231233
0.1	0.9774	12058.981	0.228596
0.2	0.9765	12234.569	0.227694
0.3	0.9759	12532.932	0.226741
0.4	0.9723	12958.821	0.225512
0.5	0.9612	13510.965	0.220454

9.0 Conclusions

The detailed linear stability analysis of Plane Poiseuille Flow (PPF) of a Casson fluid in the presence of a uniform transverse magnetic field through a porous medium has been extensively investigated. The characteristics of the basic flow are dependent on the porous parameter, and the velocity profiles reveal that porosity has an adverse effect on the fluid flow's velocity near the boundaries. Furthermore, sufficiency conditions for the resulting eigenvalue problem are derived using the Energy method, from which the qualitative behavior of the system is ascertained, showing that the system remains stable under infinitesimal disturbances.

Utilizing the Chebyshev collocation method, it is determined that there are no unstable modes when the yield stress of the Casson fluid is significant. However, an area of unstable modes emerges with an increasing Casson parameter (as shown in Table 2). The critical value of the Reynolds number decreases with the simultaneous increase in the Casson parameter, resulting in an expanded unstable region. This early onset of instability is attributed to the loss of viscosity in the Casson fluid due to high deformation rates, which, in turn, leads to increased fluid velocity. The critical values of the triplets (Re_c , α_c , c_c) obtained exhibit high accuracy and align well with the results of previous researchers.

Additionally, the neutral stability curves (Figure 4) indicate that an increase in the applied transverse magnetic field expands the stable region. This finding, however, contradicts the results observed with varying Casson parameters. On the other hand, increasing the porous parameter (Figure 5 and Table 3) consistently stabilizes the fluid flow, delaying the onset of instability by suppressing the growth rate of disturbances. Notably, both the Hartmann number and the porous parameter have similar effects on Casson fluid, but the porous parameter exhibits a slightly greater region of stabilization. The non-Newtonian Casson fluid model with high yield stress consistently enhances the stability of the flow.

The results obtained have significant relevance and practical utility within the metals, mining, and fuels sectors.

10.0 Acknowledgements

We are grateful to Ramaiah Institute Technology, Bangalore for their encouragement and support.

11.0 References

1. Drazin PG, Reild WH. Hydrodynamic Stability. Cambridge University Press. 2nd ed.
2. Tritton DJ. Physical Fluid Dynamics. Springer. 1st ed.
3. Drazin PG. Introduction to Hydrodynamic Stability. Cambridge University Press.

4. Criminale WO, Jackson TL, Joslin RD. Theory and Computation of Hydrodynamic Stability. Cambridge University Press.
5. Chandrashekar S. Hydrodynamic and Hydromagnetic Stability. Cambridge University Press. Vol. 13:1.
6. Orszag SA. Accurate solution of the Orr–Sommerfeld stability equation. Cambridge University Press. 2nd ed. Vol. 50, p. 689-703.
7. Chock DP, Schechter RS. Critical Reynolds number of the Orr-Sommerfeld equation. The Physics of Fluids. 1973; 16:329.
8. Dowell EH. Non-linear theory of unstable plane Poiseuille flow. Journal of Fluid Mechanics; Cambridge University Press. 1969; 38(2):401-414.
9. Makinde OD. On the Chebyshev collocation spectral approach to stability of fluid flow in a porous medium. International Journal for Numerical Methods in Fluids. 2009; 59(7):791-799.
10. Basavaraj MS. Instability of MHD fluid flow through a horizontal porous medium in the presence of the transverse magnetic field - A linear stability analysis. Journal of the Indian Mathematical Society. 2019; 86(3-4):241-258.
11. Mustafa M, Hayat T, Pop I, Aziz A. Unsteady boundary layer flow of a Casson fluid due to an impulsively started moving flat plate. Heat Transfer - Asian Research. 2011; 40(6):563-576.
12. Bhattacharyya K, Hayat T, Alsaedi A. Analytic solution for magnetohydrodynamic boundary layer flow of Casson fluid over a stretching/shrinking sheet with wall mass transfer. Chinese Physics B. 2013; 22(024702).
13. Nadeem S, Ul Haq R, Lee C. MHD flow of a Casson fluid over an exponentially shrinking sheet. Scientia Iranica. 2012; 19(6):1550-1553.
14. Fung YC. Biodynamics Circulation. Springer. 1st ed. 1984.
15. Boyd J, Buick JM, Green S. Analysis of the Casson and Carreau-Yasuda non-Newtonian blood models in steady and oscillatory flow using the lattice Boltzmann method. Physics of Fluids. 2007; 19:93-103.
16. Kandasamy A, Pai RG. Entrance Region Flow of Casson Fluid in a Circular Tube. Applied Mechanics and Materials. 2012; 110-116:698-706.
17. Basavaraj MS, Aruna AS, Vijayakumar, Shobha T. MHD instability of the pressure-driven plane laminar flow in the presence of the uniform coplanar magnetic field: Linear stability analysis. Heat Transfer. 2021; 50:5779-5792.
18. Aruna AS, V Kumar, Basavaraj MS. The effect of temperature/gravity modulation on finite amplitude cellular convection with variable viscosity effect. Indian Journal of Physics. 2021.
19. Basavaraj MS, Shobha T, Aruna AS. The combined effect of the porosity of the porous media and the longitudinal magnetic field on the stability of the modified plane Poiseuille flow. SADHANA - Indian Academy of Sciences. 2021;46.
20. Basavaraj MS. Instability of the plane parallel flow through a saturated porous medium in the presence of a longitudinal magnetic field using the Chebyshev collocation method. International Journal of Non-Linear Mechanics. 2021;137.
21. Asogwa KK, Ibe A. A Study of MHD Casson Fluid Flow over a Permeable Stretching Sheet with Heat and Mass Transfer. Journal of Engineering Research and Reports. 2022.
22. Reyaz R, Mohamad AQ, Lim YJ, Saqib M, Shafie S. Analytical Solution for Impact of Caputo-Fabrizio Fractional Derivative on MHD Casson Fluid with Thermal Radiation and Chemical Reaction Effects. Fractal and Fractional. 2022; 6(1):38.
23. Saravana R, Hemadri Reddy R, Narasimha Murthy KV, Makinde OD. Thermal radiation and diffusion effects in MHD Williamson and Casson fluid flows past a slendering stretching surface. Heat Transfer. 2022; 51(4):3187-3200.
24. Eswara Rao M. The effects of thermal radiation and chemical reaction on MHD flow of a Casson fluid over an exponentially inclined stretching surface. Journal of Physics: Conference Series. 2018.
25. Tunde A, Yusuf Rasaq A, Kareem, Samuel O, Adesanya, Jacob A, Gbadeyan. Entropy generation on MHD flow of a Casson fluid over a curved stretching surface with exponential space-dependent heat source and nonlinear thermal radiation. Heat Transfer. 2022; 2079-2098.
26. Kudenatti RB, Noor-E-Misbah. The onset of instability in a hydromagnetic channel flow of Casson fluid: the accurate solution. Applied Mathematics and Computation. 2023.
27. Al-Kouz W, Owhaib W. Numerical analysis of Casson nanofluid three-dimensional flow over a rotating frame exposed to a prescribed heat flux with viscous heating. Scientific Reports. 2022; 12:4256.
28. Naga Santoshi P, Ramana Reddy GV, Padma P. Numerical scrutinization of three-dimensional Casson fluid with viscous heating and prescribed heat flux using

a modified Buongiorno model. Scientific Reports. 2021; 11:2066.
29. Fusi L, Farina A, Rajagopal KR, Vergori L. Channel flows of shear thinning fluids that mimic the mechanical response of a Bingham fluid. International Journal of Non-Linear Mechanics. 2021; 138:103847.
30. Nawaz M, Rahila Naz, Awais M. Magnetohydrodynamics axisymmetric flow of Casson fluid with variable thermal conductivity and free stream. Alexandria Engineering Journal. 2018; 57:2043-2050.
31. Nield DA. The stability of flow in a channel or duct occupied by a porous medium. International Journal of Heat and Mass Transfer. 2003; 46(22):4351-4354.
32. Hill AA, Straughan B. Stability of Poiseuille Flow in a Porous Medium. Advances in Mathematical Fluid Mechanics. Springer, Berlin, Heidelberg. 2010.
33. Takashima M. The stability of the modified plane Poiseuille flow in the presence of a transverse magnetic field. Fluid Dynamics Research. 1996; 17(6):293-310.
34. Lock RC. The stability of the flow of an electrically conducting fluid between parallel planes under a transverse magnetic field. Royal Society. 1955.
35. Moler CB, Stewart GW. An algorithm for generalized matrix eigenvalue problems. SIAM Journal on Numerical Analysis. 1973; 10(2).